Desalination and Water Treatment
www.deswater.com

doi: 10.1080/19443994.2015.1109557

57 (2016) 20188–20198
September

Taylor & Francis
Taylor & Francis Group

Optimization of fabrication parameters for nanofibrous composite membrane using response surface methodology

Seong-Jik Park[a,b,*], Hee-Kyung An[a]

[a]*Department of Bioresources and Rural System Engineering, Hankyong National University, Anseong, Korea, Tel. +82 670 5131; emails: parkseongjik@hknu.ac.kr (S.-J. Park), he609@naver.com (H.-K. An)*
[b]*Institute of Agricultural Environmental Science, Hankyong National University, Anseong, Korea*

Received 14 January 2015; Accepted 13 October 2015

ABSTRACT

In this study, response surface methodology (RSM) is introduced as an efficient method for investigating and optimizing important parameters for the synthesis of an active layer on the surface of a nanofibrous midlayer. The nanofibrous composite membranes fabricated in this study comprised a polyethylenimine (PEI)/trimesoyl chloride (TMC)-active layer, electrospun polysulfone (PSf)/polyethylene glycol (PEG) midlayer, and commercial polyethylene terephthalate (PET) nonwoven mechanical support layer. The PEI/TMC-active layer was fabricated under the following conditions: 2–4 w/v% PEI, 1–3 w/v% camphor sulfonic acid (CSA), and 0.5–1.5 w/v% TMC. The effect of the three parameters on the membrane performance (i.e. permeate flux and salt rejection) in aqueous solutions containing 2,000 mg/L NaCl at 7 bar was investigated. The Box–Behnken design was used to elucidate the effects of the concentrations of PEI, CSA, and TMC on the membrane performance and optimize these parameters. The results demonstrated that PEI concentration had the most significant influence on both permeate flux and salt rejection. The highest permeate flux and ion rejection values obtained from the polynomial model were 26.83 L/m^2 h and 74.90%, respectively. Confirmation runs revealed that the predicted and experimentally obtained data were within 4.0%, indicating acceptable accuracy of the predicted model attained from the RSM study. Although further research is necessary for confirmation, our results reveal that the RSM used in this experiment could be a useful tool for optimizing parameters for cross-linking reactions and quantitatively evaluating the effect of experimental conditions on nanofiltration properties.

Keywords: Nanofiber; Nanofiltration; Response surface methodology; Optimization; Polyethylenimine

1. Introduction

Traditional methods of obtaining polymer fibers include melt spinning, spinning from a solution or liquid-crystalline state, and formation from a gel state. Recently, another method of fiber production, i.e. electrospinning, has attracted attention. Using this technique, nanofibers with diameters ranging from a few hundred nanometers to a few microns can be produced. Nanofibers produced via electrospinning have several unique characteristics such as a large surface area to unit volume ratio, high porosity (up to >80%), nano-size

*Corresponding author.

1944-3994/1944-3986 © 2015 Balaban Desalination Publications. All rights reserved.

pores, and flexibility for chemical/physical surface functionalization [1,2]. With these properties, electrospun membranes can provide good scaffolds for nanofiltration membranes with high water flux and low-energy consumption. Whereas conventional membranes produced using the phase inversion method contain many dead-end pores through which pure water cannot pass, the fully interconnected pores of electrospun nanofibrous membranes provide abundant water pathways with low hydraulic resistance [3]. Although electrospinning is applicable for the generation of both pressure-driven membranes and forward-osmosis membranes with several advantages, the active layer cannot be easily synthesized on electrospun nanofibers due to their rough surface and large pores.

Fabrication of the active layer using interfacial polymerization, which involves *in situ* polycondensation of amine and acid-chloride monomers at the interface of two immiscible solvents, has been widely adopted [4]. The effective parameters of interfacial polymerization such as the concentrations and species of amine and acid chloride monomers, solvents, reaction time, heat curing, and additives, such as surfactants, can have an extreme influence on the membrane structure and performance, i.e. permeate flux and salt rejection [5,6]. Although the current products and research for the fabrication of thin-film composite (TFC) reverse osmosis membranes are based on the original chemistry, which was discovered during the 1980s, i.e. interfacial polymerization, the performance of the TFC membranes has improved dramatically; these improvements have resulted from surface modification and close monitoring of the interfacial polymerization reaction parameters [6].

Most of the previous research on membrane fabrication and synthesis has adopted conventional methods of experimentation involving variation of one parameter, while the others are kept constant. This conventional method requires many experimental runs, which require a significant amount of time and chemicals, to determine the optimum conditions for membrane fabrication and synthesis. Using the conventional method, it is also difficult to investigate the effects of interactions between the considered process parameters [7]. These limitations can be overcome by applying a well-known statistical method, i.e. response surface methodology (RSM). RSM involves simultaneous variation of many factors over a set of experimental runs and enables elucidation of the optimized conditions and evaluation of the relative significance of several factors even in the presence of complex interactions [8,9]. A statistically designed experimental plan enables optimization and analysis of experimental factors with small experimental runs.

Statistically designed experiments and RSM have been applied successfully in various scientific and technical fields to analyze adsorption, biomass pretreatment, and mechanical processes. Over the last few years, RSM has also been successfully applied for membrane fabrication by some researchers. Xiarchos et al. [10] studied the effect of the surfactant, concentration, pH, and surfactant/metal ratio on the removal of copper from aqueous solutions using micellar-enhanced ultrafiltration with a central composite design. Chen et al. [11] applied a five-level, five-variable central composite rotatable design analysis of various factors, i.e. polymer concentration, distance, temperature, flow rate, and voltage, for the fabrication of electrospun poly (methyl methacrylate) nanofibrous membranes. Khayet et al. [7] adopted RSM to optimize the conditions for the fabrication of nanofiltration-modified membranes using UV-initiated graft polymerization. Madaeni et al. [12] presented the application of RSM for the optimization of the preparation of nanofiltration membranes via phase inversion. Razali et al. [13] used the central composite design for the optimization of blended polyethersulfone/polyaniline membranes. In all these studies, statistically based experimental designs using RSM have been proven to be effective for the optimization of experimental conditions to obtain reasonable results with small experimental runs.

To the best of our knowledge, however, no experimental study using RSM has been performed regarding the fabrication of nanofibrous composite membranes. In our previous research [14], it could be found that polyvinylidene fluoride nanofibers and polyethylene imine (PEI) were promising building blocks for the fabrication of high-performance naonofiltration membranes, but optimizing the experimental condition for improving water flux and ion rejection was not performed. Therefore, this study applies the Box–Behnken design to optimize experiments and elucidate the effect of parameters and their interactions on the fabrication of active layers on nanofibrous scaffolds. The investigated parameters include the concentrations of PEI, camphor sulfonic acid (CSA), and trimesoyl chloride (TMC) used for fabrication of the active layer on top of electrospun nanofibers.

2. Materials and methods

2.1. Chemicals

Polysulfone (PSf; P-35,00, $M_w = 7.7 \times 10^4$–8.3×10^4 g/mol, $M_n = 2.2 \times 10^3$ g/mol) and polyethylene glycol (PEG; $M_w = 600$ g/mol) were purchased from Solvay and Tokyo Chemical Industry, respectively.

Commercial poly(ethylene terephthalate) (PET) nonwoven fabric was supplied by E&H (Korea). All solvents used in this experiment, i.e. N-methyl-2-pyrrolidone (NMP; 99.5%), N,N-dimethylformamide (DMF; anhydrous, 99.5%), and n-hexane (solution, 95%), were purchased from Daejung Chemical (Korea). 1,3,5-Benzenetricarbonyl trichloride (TMC; 98%), polyethylenimine (PEI; $M_w = 2.5 \times 10^4$ g/mol, $M_n = 1.0 \times 10^4$ g/mol), and (+)-camphor-10-sulfonic acid (CSA; powder, 98.0%) were purchased from Sigma–Aldrich and used to fabricate the active layer. Sodium chloride (crystalline, 99.5%) purchased from Daejung Chemical (Korea) was dissolved in deionized water with a resistivity of 18.2 mΩ cm for the solution for cross-flow filtration.

2.2. Membrane preparation

For electrospinning, a typical polymeric dope solution was prepared by dissolving PSf (19 g) and PEG (1 g) in a mixture 80 mL of DMF and NMP (1:1 w/w); 0.1 g of NaCl was then added to the polymeric dope solution. The mixture was stirred at 80˚C for 24 h to obtain a homogeneous dope solution. The dope solution was fed into a 10-mL syringe using a Gage 20 needle (O.D. = 0.902 mm and I.D. = 0.584 mm). The syringe was fixed into a syringe pump (KDS-100, KD Scientific, US) and a rugged metal clip connected to a high-voltage supply was clipped to the needle of the syringe. The drum collector was wrapped with commercial PET nonwoven fabric. The PSf/PEG-blend scaffold was then electrospun onto the PET nonwoven fabric at a flow rate of 1.5 mL/h, voltage of 18.5 kV, needle-to-collector distance of 10.5 cm, and collector speed of 570 rpm. The nanofibers were electrospun in a chamber to control the humidity and temperature at 40% and ~18–22˚C, respectively.

A polyamide-active layer was fabricated on top of the PSf/PEG electrospun support membranes using the interfacial polymerization method. The PSf/PEG electrospun support membranes were first immersed for 5 min in PEI/CSA blend-solutions; these solutions were prepared by dissolving 2, 3, or 4 g of CSA in 100 mL of DI water under vigorous stirring followed by the dissolution of 2, 3, or 4 g of PEI into the solutions, respectively. Any excess PEI/CSA-solution was removed from the surface of the support membrane using a rubber roller. The PEI-CSA-saturated support membranes were then dipped into 0.5, 1.0, or 1.5 w/v % TMC in n-hexane for 5 min. The post-treatment process for curing the composite membrane included thermal treatment in a vacuum oven at 70˚C for 15 min followed by three rinses with DI water. Until use, the nanofibrous composite membrane was stored in DI water.

2.3. Cross-flow filtration

A custom-built filtration system with 21.84 cm^2 of effective filtration area was used to test the permeation flux and ion rejection of the nanofibrous composite membranes prepared via different experimental conditions, as schematized in Fig. 1. The loaded membrane was first compacted with DI water at an applied pressure of 7.0 bar for 1 h. NaCl was then used to investigate the ion selectivity of the nanofibrous composite membrane; 2 L of a 2,000 mg/L salt solution was used to fill the feeding tank. During the filtration experiments, the feed pressures were set at 7.0 bar. The concentration of salt in each membrane permeate was measured using an electrical conductivity (EC) meter. The permeate volume through each membrane was measured using a digital balance (EK-6100, AND, Korea), which was connected to a computer and recorded in real time. The permeate flux through each membrane was calculated by dividing the permeate volume by the effective area of membrane and the sampling time. The ion rejection and permeate flux when constant over time were used to constitute the experimental design matrix.

2.4. Membrane characterization

The contact angles of the nanofibrous composite membrane surfaces were measured using a contact-angle analyzer (Phoenix 150, SEO cooperation, Korea). A sessile drop of water was placed on the surface of the membrane using a microsyringe; the drop image was immediately captured and analyzed using an image-analyzing program. The measurement was repeated more than 10 times to obtain the average contact angle. The cross-sectional and surface morphologies of the membranes were observed using a field emission scanning electron microscope (FESEM; S-4700, Hitachi, Japan). Before the observation, all samples were coated with gold at 30 mA for 120 s to minimize the charging effect. To obtain a cross-section of the membrane, the membranes were fractured after freezing in liquid nitrogen. The chemical compositions of the top surfaces of the membranes were characterized using Fourier-transform infrared spectroscopy (FTIR, Vertex 70, Bruker, Germany) with an attenuated total reflectance (ATR) accessory. All samples were scanned from 500 to 4,000 cm^{-1} at a scanning speed of 2 mm/s. A zinc selenide ATR crystal plate was used with an aperture angle of 45˚.

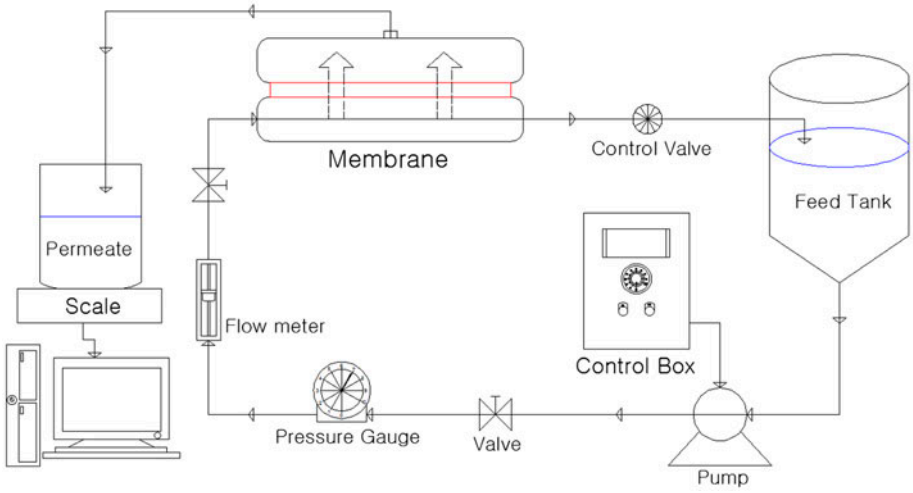

Fig. 1. Schematic diagram of cross-flow filtration experiments.

2.5. Experimental design

The optimal conditions for the fabrication of active layers on the nanofibrous scaffolds were determined and the interactions of the variables for the fabrication were evaluated using the Box–Behnken model in an RSM study. Three independent variables, i.e. the PEI, CSA, and TMC concentrations, were selected. Table 1 presents the actual levels and corresponding codes of the process variables. Overall, 15 sets of treatment combinations involving three replicates at center point were analyzed using design expert statistical software (version 7.0.0, STAT-EASE Inc., Minneapolis, MN, USA). Linear and second-order polynomials were employed to fit the experimental data obtained. The adequacy of the model was tested using the sequential *F*-test, lack-of-fit test, and other adequacy measurements.

If the response varied in a polynomial manner, it was represented using the following polynomial function equation:

$$Y = a_0 + a_1 x_1 + a_2 x_2 + a_3 x_3 + a_{12} x_1 x_2 + a_{13} x_1 x_3 + a_{23} x_2 x_3 \quad (1)$$

Table 1
Experimental design levels of chosen variables

		Coded factor level		
Variables	Symbol	−1	0	1
PEI (w/v%)	x_1	2	3	4
CSA (w/v%)	x_2	1	2	3
TMC (w/v%)	x_3	0.5	1.0	1.5

However, if there was a curvature in the system, a higher order polynomial-like quadratic model was used, which was represented using the following equation:

$$Y = a_0 + a_1 x_1 + a_2 x_2 + a_3 x_3 + a_{12} x_1 x_2 + a_{13} x_1 x_3 + a_{23} x_2 x_3 + a_{11} x_1^2 + a_{22} x_2^2 + a_{33} x_3^2 \quad (2)$$

where Y is the predicted response (i.e. permeate flux, L/m^2 h; ion rejection, %), x_i are the variables, and a_i are the model coefficient parameters. Subscripts 1, 2, and 3 refer to the PEI, CSA, and TMC concentrations, respectively. The highest order polynomial model with significant additional term and not aliased was recommended by the statistical software. Based on the recommended model, the relationship between the three independent variables and two responses was analyzed.

3. Results and discussion

3.1. Modeling

The Box–Behnken model of RSM was employed in these experiments to obtain a polynomial model from a 15-experiment design run. The ranges and levels of the three independent variables, i.e. PEI, CSA, and TMC concentrations, are shown in Table 1. *F*-value tests were performed using an analysis of variance (ANOVA) to calculate the significance of each model employed in the design expert statistical software. The results for permeate flux recommended a quadratic model as the highest order polynomial model that

satisfies that the additional terms are significant and the model is not aliased. The predicted response for permeate flux, Y_{PF}, as a function of the coefficient of independent variables of the full quadratic model was obtained as:

$$Y_{PF} = 15.26 - 5.13\,x_1 - 0.47\,x_2 + 1.11\,x_3 + 1.94\,x_1\,x_2 + 0.0085\,x_1\,x_3 + 1.14\,x_2\,x_3 + 2.84\,x_1^2 + 1.20\,x_2^2 - 2.85\,x_3^2 \quad (3)$$

where x_1, x_2, and x_3 are the coded values for the three variables, i.e. PEI, CSA, and TMC concentrations (w/v %), respectively. A two-factor interaction (2FI) model was suggested for ion rejection; the following response model equation was used:

$$Y_{IR} = 54.76 + 11.10\,x_1 + 1.70\,x_2 - 1.71\,x_3 - 9.56\,x_1\,x_2 + 0.22\,x_1\,x_3 + 1.47\,x_2x_3 \quad (4)$$

where Y_{IR} is the predicted ion rejection (%).

The significance of the values of the model equations for permeate flux and ion rejection were checked by F, R^2, adjusted R^2, lack-of-fit, and adequate precision tests. In case of the permeate flux, as shown in Table 2, the model F-value, which was calculated by dividing the mean squares of each variable effect by the mean square, was 8.43, and the low probability value (0.0151), which was less than p-value at the 95% confidence limit, verified that the model terms were significant. The model probability value (0.0034) for ion rejection was also low enough to confirm that the model terms for ion rejection were significant. The goodness-of-fits of the models were tested via the correlation coefficient R^2, which represented the real relationship among the selected factors and the percentage of the variability of the optimized parameters [12]. The R^2 value (0.938) for the permeate flux indicated that only 6.2% of the variation in the permeate flux response could not be explained by the model and the model fitted well with the observed data. The R^2 value (0.870) for ion rejection was also reasonably close to 1 and was thus acceptable. The adjusted R^2 values for permeate flux and ion rejection were 0.827 and 0.773, respectively: Both were statistically reasonable. Lack-of-fit tests were also used to evaluate the model adequacy; an insignificant lack-of-fit is desired. The lack-of-fit values for permeate flux and ion rejection were 0.1484 and 0.3493, respectively; these values were statistically insignificant and showed that the constructed models were suitable to describe the observed data. The values of adequate precision, which reflected the signal-to-noise ratio, were 10.81 and 11.80 for permeate flux and ion rejection, respectively; because these values were greater than 4, they indicated adequate signals. Fig. 2 shows that the points of the predicted vs. actual plots for permeate flux and ion rejection were clustered along a diagonal line, indicating that the predicted values matched well with the observed ones.

3.2. Effect of PEI, CSA, and TMC concentrations on water flux

The permeate-flux variations of the fabricated NFC membranes with different PEI, CSA, and TMC concentrations are shown in the response surface of Fig. 3. As can be seen from Fig. 3(a) and (c), the permeate flux of the NFC membrane decreased with increasing PEI concentration; this reduction was also observed in the model equation of permeate flux. Table 2 shows that a statistical analysis of the experimental range of this study identified the PEI concentration as the most significant factor for the permeate flux. The p-value of less than 0.05 indicated the significance of the model term. The negative sign of the coefficient of x_1 and x_1^2 in the model equation for permeate flux indicated that the permeate flux decreased with increasing PEI concentration. As is well known, increasing amine monomer concentration causes the formation of a thicker active layer. Similar results were also reported by Saha and Joshi [5]. An increase in the piperazine concentration up to 1.5 w/v% at constant TMC concentration decreased the water flux but increased ion rejection. The active layer became thicker until the monomers diffusing through the active layer were consumed by other monomers and/or functional groups [5,15]. The amine monomer diffused into the organic phase and generated the thick membrane perpendicular to interface, which reduced the permeate flux [16].

In contrast to the effect of PEI concentration, the effects of the CSA and TMC concentrations on the permeate flux were statistically negligible: The p-values of x_2 and x_3 were more than 0.05, which indicated the insignificance of these model terms, as shown in Table 2. CSA has been commonly used as an additive together with trimethylamine (TEA) to remove the hydrogen chloride formed during amide-bond formation [17–19]. These researchers reported that membranes prepared with TEA and CSA had a higher permeability without compromising salt rejection than those prepared without TEA and CSA. However, our preliminary experiments showed that the active layer prepared with both TEA and CSA was delaminated

Table 2
ANOVA for response surface model ANOVA

	Water flux (L/m^2 h)					Ion rejection (%)				
Source	Sum of squares	df	Mean Square	*F*-value	*p*-value Prob. > *F*	Sum of squares	df	Mean square	*F*-value	*p*-value Prob. > *F*
Model	312.31	9	34.70	8.43	0.0151	1,408.27	6	234.71	8.93	0.0034
x_1	210.26	1	210.26	51.07	0.0008	986.35	1	986.35	37.55	0.0003
x_2	1.75	1	1.75	0.43	0.5431	22.88	1	22.88	0.87	0.3780
x_3	9.92	1	9.92	2.41	0.1812	23.46	1	23.46	0.89	0.3723
x_1x_2	15.00	1	15.00	3.64	0.1145	366.72	1	366.72	13.96	0.0057
x_1x_3	0.03	1	0.03	0.01	0.9365	0.19	1	0.19	0.01	0.9344
x_2x_3	5.22	1	5.22	1.27	0.3112	8.67	1	8.67	0.33	0.5814
x_1^2	29.74	1	29.74	7.22	0.0434					
x_2^2	5.32	1	5.32	1.29	0.3071					
x_3^2	30.02	1	30.02	7.29	0.0428					
Residual	20.59	5	4.12			210.16	8	26.27		
Lack-of-fit	18.49	3	6.16	5.90	0.1484	182.12	6	30.35	2.16	0.3493
Pure error	2.09	2	1.05			28.04	2	14.02		
Cor total	332.90	14				1,618.44	14			

by shear stress from cross flow. Therefore, we synthesized the active layer on the nanofibrous support layer without TEA. Ghosh et al. [19] evaluated the independent role of CSA on the polycondensation reaction between amine and acid-chloride monomers and reported that CSA effectively inhibited shrinkage of the microporous skin layer of the support membrane during heat curing. The results concur with the other literature [20], which adopted the use of CSA in the polycondensation reaction to avoid the loss of flux during the heat treatment of a polyamide thin film. In contrast to the membrane with a midlayer formed by phase inversion used by Ghosh et al. [19], the midlayer used in this study was made of electrospun nanofibers with large pores, indicating that the decrease in permeate flux due to shrinkage of the pores of the electrospun layer was insignificant. Yu et al. [21] suggested other reason for the use of CSA, which was added to amine solution to adjust the pH of the solution.

In contrast to the effect of PEI concentration on permeate flux, the effect of TMC concentration was not statistically significant. A similar phenomenon was observed by Roh et al. [22] who fabricated a TFC membrane with m-phenylenediamine (MPD) and TMC using interfacial polymerization. The water flux decreased by 3% with increasing TMC concentration from 0.01 to 0.1 w/v% and remained almost constant at higher TMC concentrations. However, the water flux decreased by 24% as the MPD concentration increased from 0.01 to 0.1 w/v% and decreased by 14% above 0.1 w/v% MPD. They reported that increasing the MPD concentration resulted in a thicker active layer and decreased hydrophilicity, while increasing the TMC concentration increased both the active layer thickness and hydrophilicity. Since these two parameters have counter-balancing effects on permeate flux, the decrease in permeate flux with increasing MPD concentration was greater than that with increasing TMC concentration. Our results were also in agreement with the findings of Chai and Krantz [23] who reported that interfacial polymerization was controlled by TMC diffusion at low TMC concentrations (<0.01%) and controlled by the MPD concentration at higher TMC concentrations (>0.1%). It can be inferred from their study that the interfacial polymerization process in the current study was controlled by PEI diffusion, indicating that the TMC concentration insignificantly influenced the membrane performance.

3.3. Effects of PEI, CSA, and TMC concentrations on ion rejection

Table 2 shows that the ion rejection as well as the permeate flux significantly depended on the concentration of PEI. The x_1*p*-value of 0.0003 and x_1x_2*p*-value of 0.0057 indicated the large significance of the corresponding coefficients. The positive effect of x_1 in the regression equation of ion rejection indicated that ion rejection increased at high PEI concentrations. According to the

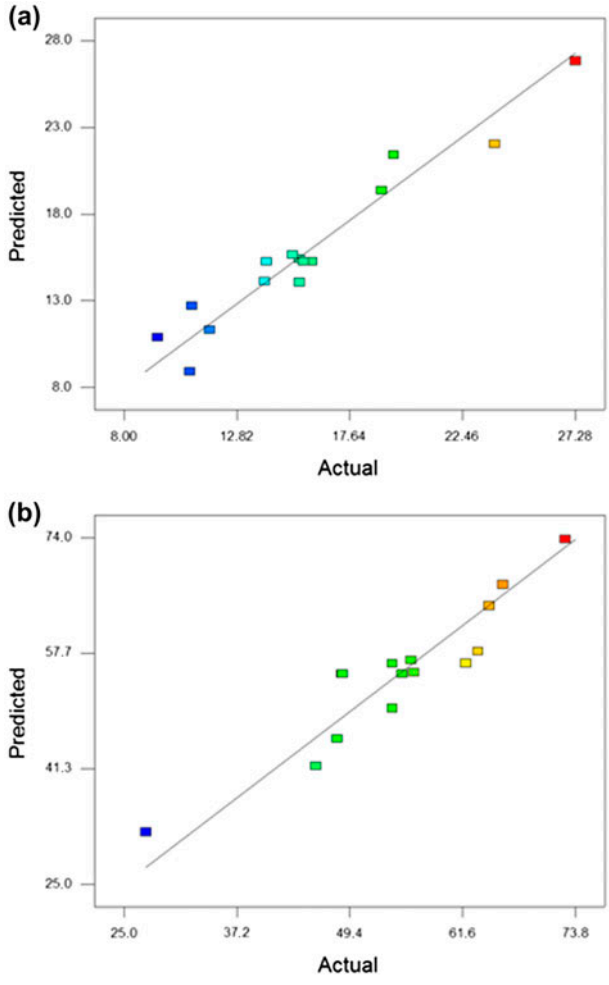

Fig. 2. Plot of predicted values vs. actual values for (a) permeate flux (L/m^2 h) and (b) ion rejection (%).

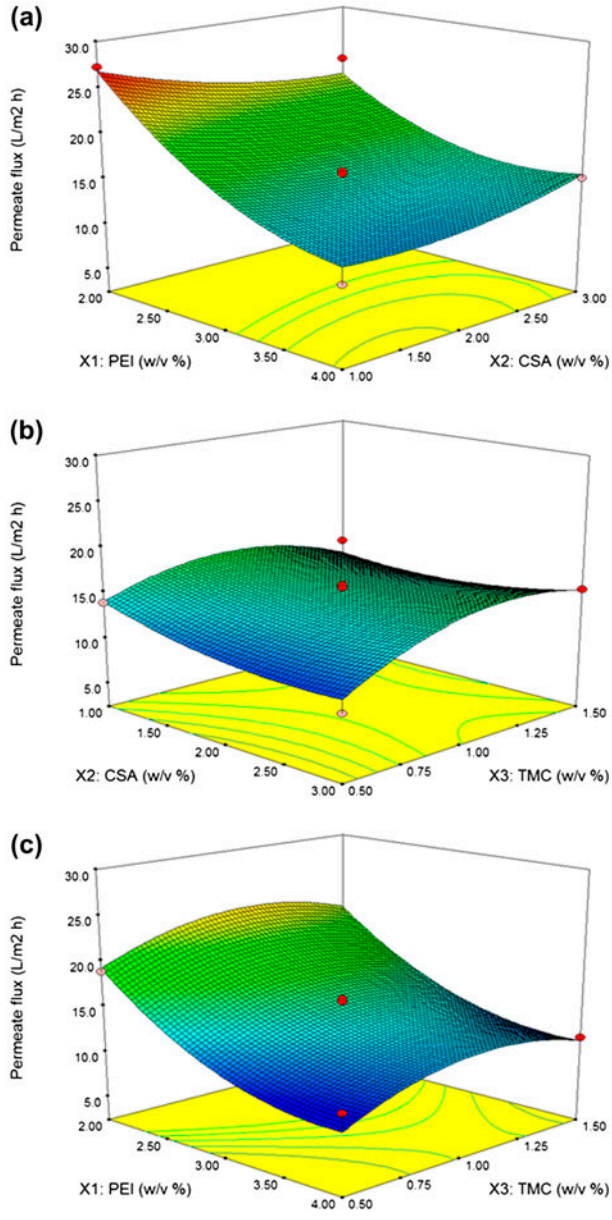

Fig. 3. Estimated response surface for permeate flux (L/m^2 h) showing the influence of (a) PEI and CSA concentrations, (b) CSA and TMC concentrations, and (c) TMC and PEI concentrations.

"solution-diffusion" model [22,24], the salt rejection was independent of the thickness of the active layer, while the water flux was inversely proportional to the thickness of the active layer. This dependence suggests that the ion rejection was primarily affected by factors other than the active layer thickness. The growth of the membrane perpendicularly to the interface between the aqueous and organic phases via amine monomer diffusion into the organic phase was followed by a heavy cross-linking reaction [16]. Unreacted COCl groups in the polyamide chains were consumed by cross-linking with amine monomers, resulting in the formation of a dense active layer with high selectivity.

As was discussed in the previous section, the PEI concentration significantly influenced the permeate flux, while the TMC concentration did not. The statistical results obtained from ANOVA analysis showed that the TMC concentration did not affect either the ion rejection or water flux of the NFC membrane. These results were attributed to the fact that the TMC concentration ranges in this study exceeded the critical value that noticeably influences the membrane performance. Song et al. [16] observed that NaCl rejection of the polyamide membrane increased appreciably with increasing TMC concentration from 0.1 to 0.35 w/v% but remained constant as the TMC concentration increased from 0.35 to 0.55 w/v%. A similar observation was also

reported by Roh et al. [22], wherein the salt rejection increased slightly as the TMC concentration increased from 0.01 to 0.1 w/v% but remained unchanged at higher TMC concentrations.

In addition to the primary influences of the individual parameters, the synergistic effects of PEI and CSA concentrations on ion rejection were investigated. Fig. 4 shows response surface curves of ion rejection plotted against two experimental factors with the other factor fixed at its intermediate value. The effects of the PEI and CSA concentrations on ion rejection, at a TMC concentration of 1.0 w/v%, are shown in Fig. 4(a): The ion rejection of the prepared membrane with 2% PEI decreased with increasing CSA concentration. However, at 4% PEI, the ion rejection of the NFC membrane was enhanced by increased CSA concentration.

3.4. Optimization

Response surface optimization was performed to maximize the two responses, i.e. permeate flux and ion rejection. To determine the obtained optimal points, confirmation experiments were performed using the experimental conditions reported in Table 3. Furthermore, the predicted and experimental results were compared and the residual and percentage of error values were calculated. The highest permeate flux of 26.83 L/m^2 h was obtained at 2.00 w/v% PEI, 1.00 w/v% CSA, and 0.99 w/v% TMC; the observed permeate flux was 27.28 L/m^2 h with 27.4% ion rejection. The maximum ion rejection of the synthesized membrane obtained from the RSM model was 74.90% at 4.00 w/v% PEI, 1.01 w/v% CSA, and 0.76 w/v% TMC; the experimentally obtained maximum ion rejection was 72.34% with 9.44 L/m^2 h. The errors (%) between the predicted and observed response values were acceptable and were within 4%.

The surface morphologies of the membranes with the highest water flux and highest ion rejection were visualized by high-resolution FESEM; the results are shown in Fig. 5. As expected, it is evident from the cross-section FESEM images that the membrane with high flux was much thinner than the membrane with high rejection. As shown in Fig. 5(a) and (b), the membrane with high ion rejection contained many tightly packed, nodular structures, which increased the surface area resulting in increased water flux. The contact angle of the membrane with the highest ion rejection was 32.8° ± 2.0°, which was lower than that (45.3° ± 2.3°) of the membrane with the highest water flux; this was because the high concentration of amphiphilic polymers, such as PEI, in the interfacial

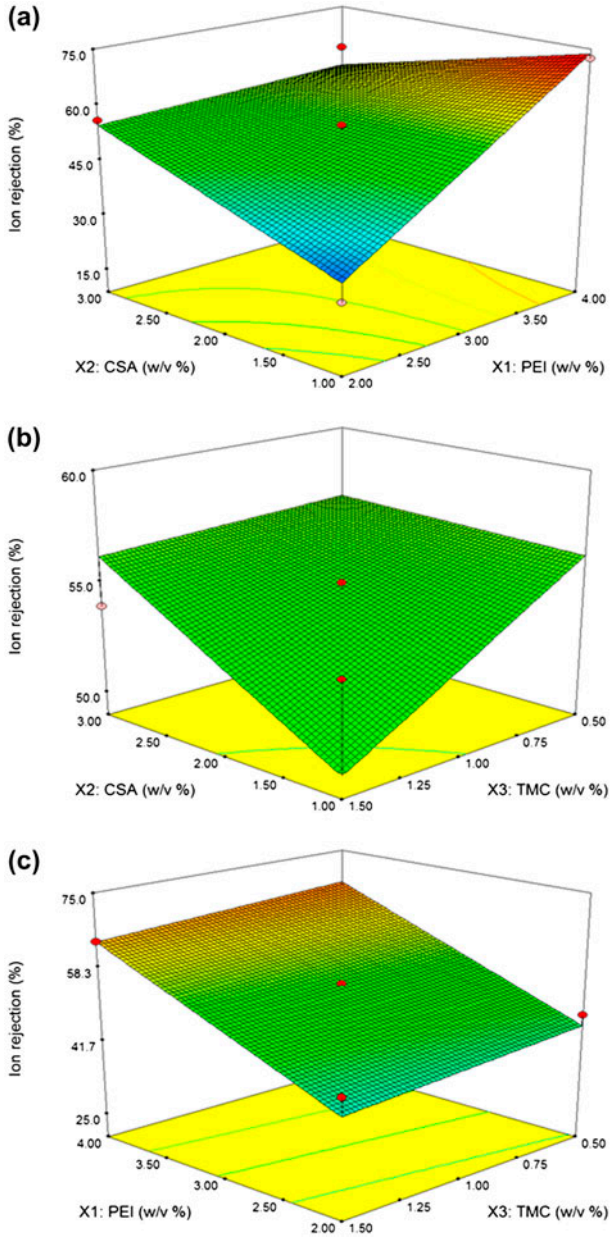

Fig. 4. Estimated response surface for ion rejection (%) showing the influence of (a) PEI and CSA concentrations, (b) CSA and TMC concentrations, and (c) TMC and PEI concentrations.

polymerization reaction increased the hydrophilicity of the membrane surface [25]. It can be inferred from these results that the permeability of the membrane was more dependent on the membrane structure than the hydrophilicity of the membrane. Fig. 6 shows the FT-IR spectra, which included bands corresponding to both the polyamide skin top layer and polysulfone sublayer of two membranes synthesized under

Table 3
RSM optimization results

Maximized Response	PEI (w/v%)	CSA (w/v%)	TMC (w/v%)	Predicted Y	Observed Y	Error (%)
Permeate flux	2.00	1.00	0.99	26.83 L/m^2 h	27.28 L/m^2 h	1.65
Ion rejection	4.00	1.01	0.76	74.90%	72.34%	3.42

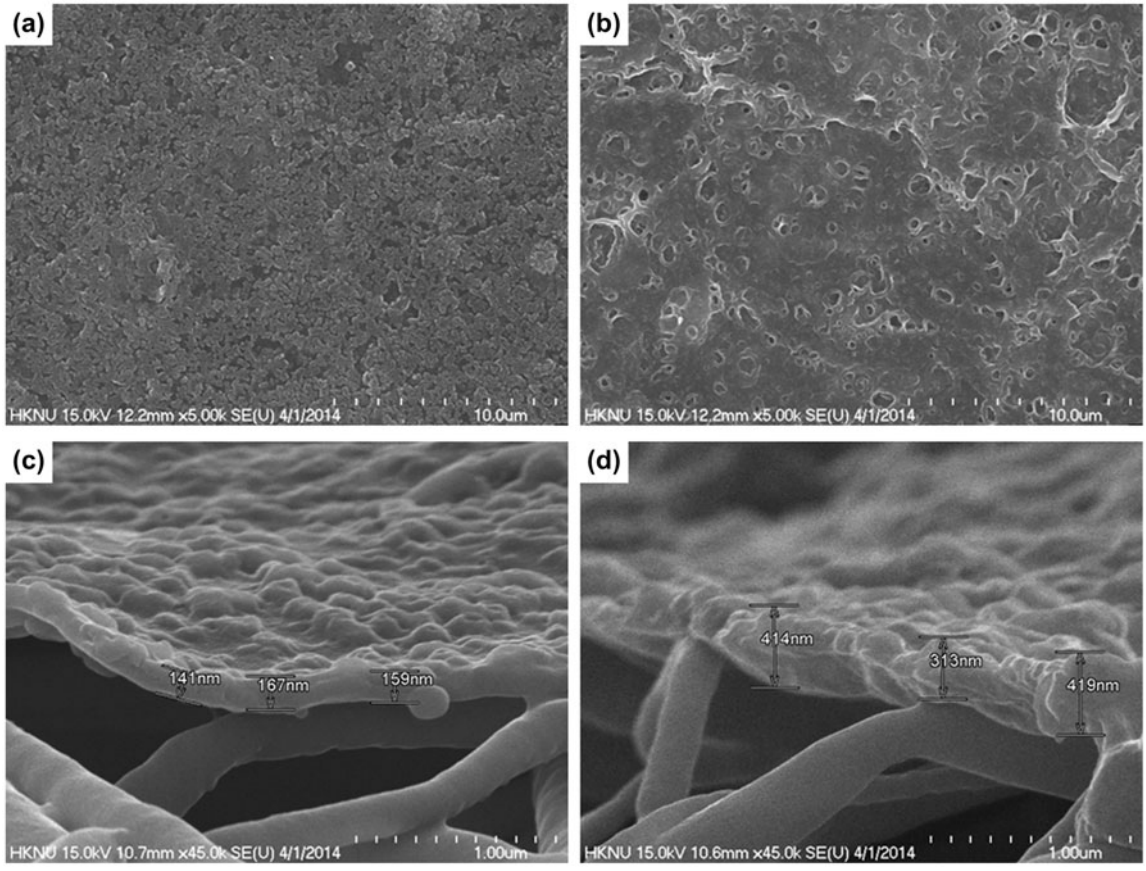

Fig. 5. FESEM images of the surfaces and cross-section morphologies of the membranes with (a, c) highest permeate flux and (b, d) highest ion rejection.

different experimental conditions. The FT-IR spectra in Fig. 6 featured some characteristic peaks for polysulfone, including aromatic in-plane bend stretching vibrations (1,581, 1,500, and 1,485 cm^{-1}), C–H symmetric deformation vibrations of $C(CH_3)_2$ (1,385 and 1,377 cm^{-1}), a C–O–C asymmetric stretching vibration (1,240 cm^{-1}), and asymmetric and symmetric SO_2 stretching vibrations (1,350–1,280 and 1,180–1,145 cm^{-1}) [26,27]. Information regarding the composition of the polysulfone midlayer could be obtained from FT-IR analysis because the penetration depth is greater than 300 nm at wave numbers <2000 cm^{-1} [27]. The peaks at 1,637 and 1,404 cm^{-1} corresponded to C=O and C–N stretches, respectively [26,28], confirming that cross-linking occurred. The amide groups were generated via cross-linking of PEI and TMC molecules.

4. Conclusion

An active layer was successfully fabricated on the surface of electrospun nanofibers using PEI and TMC via interfacial polymerization. The effect of varying the PEI, CSA, and TMC concentrations during active layer formation and optimization of these parameters were studied using the Box–Behnken model in an RSM

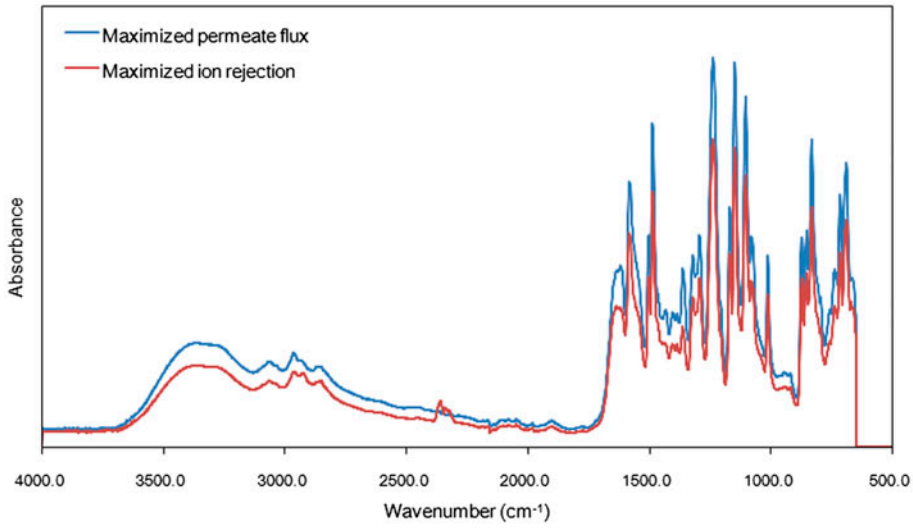

Fig. 6. ATR-FTIR spectra of the membranes with highest permeate flux and ion rejection.

study. On the basis of ANOVA analysis, the PEI concentration was determined to significantly influence both the permeate flux and ion rejection, i.e. the permeate flux decreased and ion rejection increased as the PEI concentration increased. In contrast to the influence of the PEI concentration, the concentration of TMC, which undergoes an interfacial polymerization reaction with PEI, was insignificant with respect to the membrane performance; this is attributed to the fact that the TMC concentration ranges in this study exceeded the critical value that significantly influences the membrane performance. Interactions between the PEI and CSA concentrations had an evident effect on ion rejection. By applying the polynomial model, the maximum permeate flux and ion rejection were predicted and confirmed experimentally. In the range of the factors studied, the maximum permeate flux was 26.83 L/m^2 h at 2.00 w/v% PEI, 1.00 w/v% CSA, and 0.99 w/v% TMC, whereas the maximum ion rejection was 74.90% at 4.00 w/v% PEI, 1.01 w/v% CSA, and 0.76 w/v% TMC. Comparison of the predicted and experimental results indicates an acceptable accuracy of the predicted model obtained from the RSM study. Therefore, RSM can be used to investigate the primary and interaction effects of parameters and optimize these parameters for membrane fabrication with fewer experimental trials and reduced consumption of chemicals.

Acknowledgments

This research was supported by Basic Science Research Program through the National Research Foundation of Korea (NRF) funded by the Ministry of Science, ICT & Future Planning (Project No. 2012R1A1A1014900) and. This work was also financed by a grant from the International Collaborative R&D Program of the Korea Institute of Energy Technology Evaluation and Planning (KETEP) funded by the Korean Ministry of Knowledge Economy (Project No. 20128520100020).

References

[1] T. Uyar, F. Besenbacher, Electrospinning of uniform polystyrene fibers: The effect of solvent conductivity, Polymer 49 (2008) 5336–5343.
[2] K. Yoon, B.S. Hsiao, B. Chu, Functional nanofibers for environmental applications, J. Mater. Chem. 18 (2008) 5326–5334.
[3] K. Yoon, B.S. Hsiao, B. Chu, High flux ultrafiltration nanofibrous membranes based on polyacrylonitrile electrospun scaffolds and crosslinked polyvinyl alcohol coating, J. Membr. Sci. 338 (2009) 145–152.
[4] R.J. Petersen, Composite reverse osmosis and nanofiltration membranes, J. Membr. Sci. 83 (1993) 81–150.
[5] N.K. Saha, S.V. Joshi, Performance evaluation of thin film composite polyamide nanofiltration membrane with variation in monomer type, J. Membr. Sci. 342 (2009) 60–69.
[6] K.P. Lee, T.C. Arnot, D.A. Mattia, A review of reverse osmosis membrane materials for desalination—Development to date and future potential, J. Membr. Sci. 370 (2011) 1–22.
[7] M. Khayet, M.N. Seman, N. Hilal, Response surface modeling and optimization of composite nanofiltration modified membranes, J. Membr. Sci. 349 (2010) 113–122.
[8] D.C. Montgomery, Design and Analysis of Experiments, fifth ed., John Wiley & Sons, New York, NY, 2001.

[9] R.H. Myers, D.C. Montgomery, Response Surface Methodology: Process and Product Optimization Using Designed Experiments, second ed., John Wiley & Sons, New York, NY, 2002.
[10] I. Xiarchos, A. Jaworska, G. Zakrzewska-Trznadel, Response surface methodology for the modelling of copper removal from aqueous solutions using micellar-enhanced ultrafiltration, J. Membr. Sci. 321 (2008), 222–231.
[11] J.P. Chen, K.H. Ho, Y.P. Chiang, K.W. Wu, Fabrication of electrospun poly(methyl methacrylate) nanofibrous membranes by statistical approach for application in enzyme immobilization, J. Membr. Sci. 340 (2009) 9–15.
[12] S.S. Madaeni, N. Arast, F. Rahimpour, Y. Arast, Fabrication optimization of acrylonitrile butadiene styrene (ABS)/polyvinylpyrrolidone (PVP) nanofiltration membrane using response surface methodology, Desalination 280 (2011) 305–312.
[13] N.F. Razali, A.W. Mohammad, N. Hilal, C.P. Leo, J. Alam, Optimisation of polyethersulfone/polyaniline blended membranes using response surface methodology approach, Desalination 311 (2013) 182–191.
[14] S.J. Park, R.K. Cheedrala, M.S. Diallo, C. Kim, I.S. Kim, W.A. Goddard III, Nanofiltration membranes based on polyvinylidene fluoride nanofibrous scaffolds and crosslinked polyethyleneimine networks, J. Nanopart. Res. 14 (2012) 884.
[15] R. Nadler, S. Srebnik, Molecular simulation of polyamide synthesis by interfacial polymerization, J. Membr. Sci. 315 (2008) 100–105.
[16] Y. Song, P. Sun, L.L. Henry, B. Sun, Mechanisms of structure and performance controlled thin film composite membrane formation via interfacial polymerization process, J. Membr. Sci. 251 (2005) 67–79.
[17] M.M. Chau, W.G. Light, H.C. Chu, Dry high flux semipermeable membranes, US Patent No. 4,983,291. 1997.
[18] M.A. Kuehne, R.Q. Song, N.N. Li, R.J. Petersen, Flux enhancement in TFC RO membranes, Environ. Prog. 20 (2001) 23–26.
[19] A.K. Ghosh, B.H. Jeong, X. Huang, E. Hoek, Impacts of reaction and curing conditions on polyamide composite reverse osmosis membrane properties, J. Membr. Sci. 311 (2008) 34–45.
[20] J.E. Cadotte, D.A. Batzel, T.F. Stocker, Interfacially contacting aqueous solution of polyamine monomer containing inorganic ammonium salt of acid with solution of polyfunctional acyl halide monomer in non-polar organic solvent, heating membrane to remove solvent, US Patent No. 5,658,460, 1997.
[21] S. Yu, M. Ma, J. Liu, J. Tao, M. Liu, C. Gao, Study on polyamide thin-film composite nanofiltration membrane by interfacial polymerization of polyvinylamine (PVAm) and isophthaloyl chloride (IPC), J. Membr. Sci. 379 (2011) 164–173.
[22] I.J. Roh, A.R. Greenberg, V.P. Khare, Synthesis and characterization of interfacially polymerized polyamide thin films, Desalination 191 (2006) 279–290.
[23] G.Y. Chai, W.B. Krantz, Formation and characterization of polyamide membranes via interfacial polymerization, J. Membr. Sci. 93 (1994) 175–192.
[24] J.G. Wijmans, R.W. Baker, The solution-diffusion model: A review, J. Membr. Sci. 107 (1995) 1–21.
[25] Y.F. Yang, L.S. Wan, Z.K. Xu, Surface hydrophilization of microporous polypropylene membrane by the interfacial crosslinking of polyethylenimine, J. Membr. Sci. 337 (2009) 70–80.
[26] Y.N. Kwon, J.O. Leckie, Hypochlorite degradation of crosslinked polyamide membranes II. Changes in hydrogen bonding behavior and performance, J. Membr. Sci. 282 (2006) 456–464.
[27] C.Y. Tang, Y.N. Kwon, J.O. Leckie, Effect of membrane chemistry and coating layer on physiochemical properties of thin film composite polyamide RO and NF membranes: I. FTIR and XPS characterization of polyamide and coating layer chemistry, Desalination 242 (2009) 149–167.
[28] J.B. Lambert, H.F. Shurvell, D.A. Lightner, R.G. Cooks, Introduction to Organic Spectroscopy, Macmillan, New York, NY, 1987.